Dynamics of the $Q_2\,^1\Pi_u(1)$ state studied from the isotope effect on the cross sections for the formation of the $2p$ atom pair in the photoexcitation of H_2 and D_2

Kouichi Hosaka,[1,*] Kennichi Shiino,[1] Yuko Nakanishi,[1] Takeshi Odagiri,[2] Masashi Kitajima,[1] and Noriyuki Kouchi[1]

[1]*Department of Chemistry, Tokyo Institute of Technology, Meguro-ku, Tokyo 152-8551, Japan*

[2]*Department of Materials and Life Sciences, Sophia University, Chiyoda-ku, Tokyo 102-8554, Japan*

(Received 3 February 2016; revised manuscript received 16 May 2016; published 27 June 2016)

The absolute values of the cross section for formation of a $2p$ atom pair in the photoexcitation of H_2 and D_2 are measured against the incident photon energy in the range of doubly excited states by means of the coincidence detection of two Lyman-α photons. The cross-section curves are explained only by the contribution of the doubly excited $Q_2\,^1\Pi_u(1)$ state. The isotope effect on the oscillator strengths of $2p+2p$ pair formation for H_2 and D_2 from the $Q_2\,^1\Pi_u(1)$ state is almost the same as that on the oscillator strengths of $2s+2p$ pair formation from the $Q_2\,^1\Pi_u(1)$ state obtained by our group [T. Odagiri *et al.*, Phys. Rev. A **84**, 053401 (2011)]. This channel independence indicates that both isotope effects are dominated by the early dynamics of the $Q_2\,^1\Pi_u(1)$ state, before reaching the branching point into $2p+2p$ pair formation and $2s+2p$ pair formation.

DOI: 10.1103/PhysRevA.93.063423

I. INTRODUCTION

Atomic and molecular doubly excited states are embedded in an ionization continuum, unlike excited electronic states below the ionization energy. Because of the mixing between discrete and continuum electronic states, doubly excited states of molecules are not described by Born-Oppenheimer products [1,2]. The dynamics of doubly excited molecules have thus been an attractive subject for research, in particular, for hydrogen molecules (see, for example, Refs. [3–6]). The potential energy curves and resonance widths of doubly excited states of hydrogen molecules have been calculated [7–12]. However, the dynamics of molecular doubly excited states are not fully understood even for the simplest neutral molecule, hydrogen. For example, a peak due to a forbidden doubly excited state was observed in the electron energy loss spectra of H_2 and D_2 tagged with $2p$ atom formation by our group [13,14], but the origin of the peak remains an open question [15,16]. Hence study of the dynamics of various doubly excited states of hydrogen molecules experimentally and theoretically is greatly needed. The doubly excited states of hydrogen molecules built on the $2p\sigma_u$ and $2p\pi_u$ ionic states are referred to as the Q_1 and Q_2 states, respectively, as shown in Fig. 1. Q_1 and Q_2 states with the same symmetry are numbered $1,2,3,\ldots$ in order of potential energy. For example, the $Q_2\,^1\Pi_u(1)$ state is the lowest Q_2 state with $^1\Pi_u$ symmetry, the $Q_2\,^1\Pi_u(1)$ state is the second-lowest Q_2 state with $^1\Pi_u$ symmetry, and so forth. Q_2 states correlate with the pair of excited hydrogen atoms, while Q_1 states do not.

From the experimental side the key to observing doubly excited molecules is measuring cross sections free of ionization against the excitation energy since the ionization makes a large contribution that prevents doubly excited states from being observed [13]. Odagiri *et al.* [18] developed an excellent means of investigating molecular doubly excited states, called the $(\gamma,2\gamma)$ method, along these lines. In the $(\gamma,2\gamma)$ experiment on H_2 [18], the cross section for the process

$$\begin{aligned} H_2 + \gamma_{ex} &\rightarrow H_2{}^{**} \rightarrow H(2p) + H(2p) \\ &\rightarrow H(1s) + H(1s) + \gamma_{Ly\text{-}\alpha} + \gamma_{Ly\text{-}\alpha} \end{aligned} \quad (1)$$

is measured against the energy of the incident photon γ_{ex}. In process 1, $\gamma_{Ly\text{-}\alpha}$ is a Lyman-α photon. No contribution of ionization is involved in the cross section of process 1. They [18] measured the relative values of the angle-differential cross section for emission of the Lyman-α photon pair against the incident photon energy and concluded from the reflection approximation and semiclassical treatment of the decay of doubly excited states that the intermediate state in process 1, $H_2{}^{**}$, is the doubly excited $Q_2\,^1\Pi_u(1)$ state. The isotope effect on the cross sections of process 1 is expected since neutral dissociation competes with electronic autoionization from the $Q_2\,^1\Pi_u(1)$ state. The rate of electronic autoionization has no isotope effect but the relative velocity in neutral dissociation becomes slower with heavier isotope substitution. It is hence significant to know the isotope effect on the cross section of process 1, which is a character of the doubly excited $Q_2\,^1\Pi_u(1)$ state.

In the present investigation we measure the angle-differential cross sections for the emission of a Lyman-α photon pair, process 1, against the incident photon energy with the emission angles held fixed in the photoexcitation of D_2 by the $(\gamma,2\gamma)$ method. The same measurements are carried out for H_2. We aim at obtaining the isotope effect on the cross sections of process 1. The sensitivity of the photon detectors is enhanced and the means of measuring the flux of the incident photon beam is improved so that results more accurate than those of Odagiri *et al.* [18] are obtained. We then obtain the absolute values of the angle-integrated cross sections for formation of a $2p$ atom pair in H_2 and D_2 against the incident photon energy and discuss the dynamics of the $Q_2\,^1\Pi_u(1)$ state in terms of the isotope effect on the cross section of process 1. Figure 1 shows the calculated potential energy and resonance width of the doubly excited $Q_2\,^1\Pi_u(1)$ state against the internuclear distance together with those of the $Q_2\,^1\Pi_u(2)$ state. Both states are related to the formation of a pair of excited hydrogen atoms with the principle quantum

*hosakak@chem.titech.ac.jp

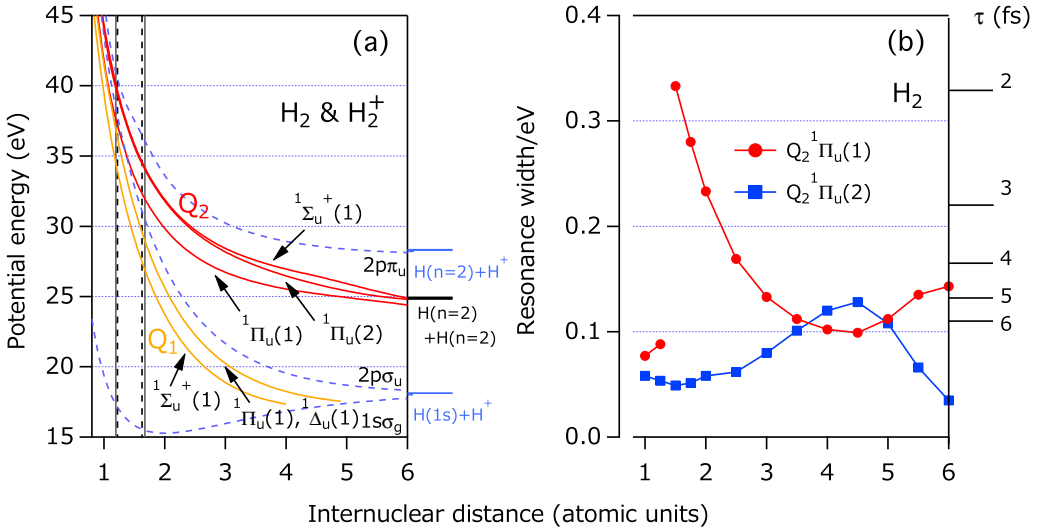

FIG. 1. (a) Potential energy curves of the doubly excited $Q_2\,{}^1\Pi_u(1)$, $Q_2\,{}^1\Pi_u(2)$, and $Q_2\,{}^1\Sigma_u^+(1)$ states of H_2 molecules (solid curves) [9] together with those of H_2^+ ions (dashed curves) [17]. Potential energy curves of the $Q_1\,{}^1\Sigma_u^+(1)$, $Q_1\,{}^1\Pi_u(1)$, and $Q_1\,{}^1\Delta_u(1)$ states [8] are also shown (solid curves). The curves of the $Q_1\,{}^1\Pi_u(1)$ and $Q_1\,{}^1\Delta_u(1)$ states are so close that they are not distinguishable. Zero energy is taken at the lowest rotational-vibrational level of the $X\,{}^1\Sigma_g^+$ state of H_2. Note that the potential energy curves of H_2 and H_2^+ are the same as those of D_2 and $D_2{}^+$, respectively. The Franck-Condon regions are seen for H_2 (solid vertical line) and D_2 (dashed vertical line). (b) Resonance widths of the doubly excited $Q_2\,{}^1\Pi_u(1)$ and $Q_2\,{}^1\Pi_u(2)$ states of H_2 as a function of the internuclear distance [9]. The right axis shows the autoionization lifetime derived from the uncertainty principle. Note that the resonance width has no isotope effect.

number 2 [18,19]. The potential energy curves of some other doubly excited states are also shown in Fig. 1(a).

II. EXPERIMENT

A schematic of the apparatus is shown in Fig. 2. Experiments were performed at BL20A [20] of the Photon Factory, Institute of Materials Structure Science, KEK. Linearly polarized light was introduced into a gas cell filled with H_2 or D_2 gas. The pair of Lyman-α photons was detected in coincidence by two detectors mounted on the wall of a gas cell and two-photon coincidence time spectra were obtained, an example of which is shown in Fig. 3. The decay times on both sides are in good agreement with the lifetime of the $2p$ state, 1.6 ns [22]. The coincidence time spectra were analyzed following the procedure described in Ref. [21] to obtain the two-photon coincidence counts. The contribution of the cascade from states $n \geqslant 3$ to the $2p$ state is not included in the coincidence counts. Measurements were carried out in the range of the incident photon energy, 30–40 eV, with the bandpass of the wavelength being 0.14 nm (energy width of 140 meV at an incident photon energy of 35 eV).

Pressure in the gas cell was lower than approximately 2 Pa for H_2 and D_2 over the present range of the incident photon energy. The pressure variation during the coincidence measurement at each photon energy was less than 1% for H_2 and D_2. It was observed that the two-photon coincidence count rate is proportional to the deuterium gas pressure up

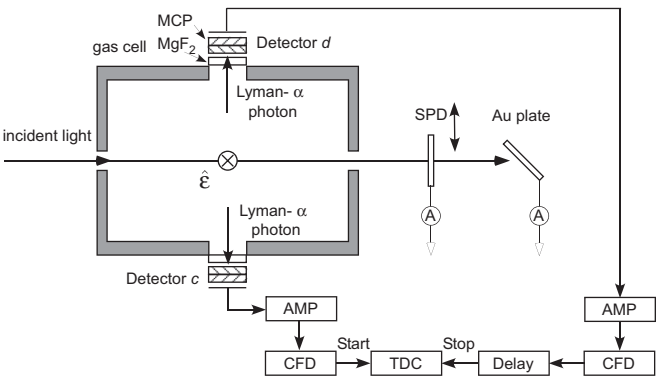

FIG. 2. Schematic of the apparatus. $\hat{\varepsilon}$: Unit polarization vector of the incident light. A, ammeter; AMP, amplifier; CFD, constant-fraction discriminator; MCP, microchannel plate; SPD, movable Si photodiode; TDC, time-to-digital converter.

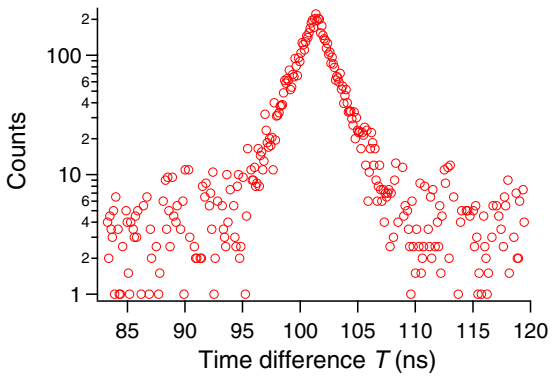

FIG. 3. Example of the two-photon coincidence time spectra, which was measured at a 33.66-eV incident photon energy and 1.1-Pa H_2 gas pressure. The accidental coincidence has been subtracted following the method described in Ref. [21]. The four channels of the time-to-digital converter are binned to be 0.1004 ns/channel. The vertical scale is logarithmic.

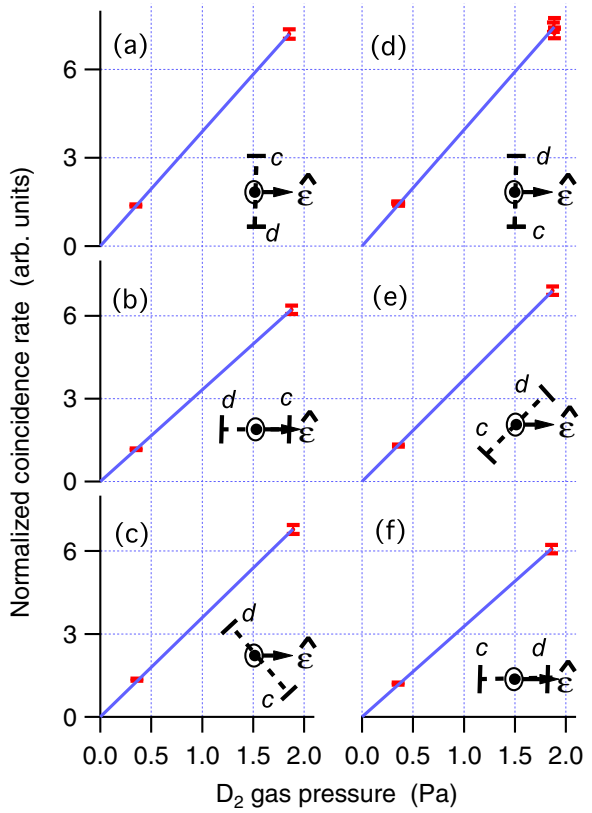

FIG. 4. Plot of the two-photon coincidence count rate against the D_2 gas pressure in the gas cell, where the coincidence count rate is normalized for the incident photon flux. The coincidence measurement was carried out at the incident photon energy of 34.86 eV. The solid line is the best-fit curve of the proportional relation. Both photon detectors are on the plane perpendicular to the incident light beam and are labeled c and d (see Fig. 2). The arrangements of the detectors are shown, where $\hat{\varepsilon}$ is the unit polarization vector of the incident light.

to ca. 2 Pa as shown in Fig. 4, which seems also to be the case for H_2. It is concluded from Figs. 3 and 4 that the two-photon coincidence counts are free of the reactions $H(n=2)+H_2[D(n=2)+D_2]$ in the present range of the target gas pressure; i.e., the coincidence counts are attributed to the primary pair of Lyman-α photons in process 1. The effect of the target gas pressure on the two-photon coincidence time spectra is discussed in detail in Ref. [21].

The flux of incident photons was measured at the exit of the gas cell using a Au plate. The sensitivity of the Au plate against the incident photon energy was obtained with a NIST-calibrated silicon photodiode [23] separately from the coincidence experiments. In the early experiment by Odagiri *et al.* [18], the flux of the incident photons was measured using a Au mesh, the sensitivity of which was obtained with the combination of sodium salicylate and a photomultiplier tube.

Each photon detector for the vacuum ultraviolet radiation is comprised of a MgF_2 window and microchannel plate [24] coated with CsI, which provides a filter range of approximately 115–200 nm. Only Lyman-α fluorescence, with a 121.6-nm wavelength, is detected in the present range of incident photon energy, 30–40 eV. Both photon detectors are on the plane perpendicular to the incident light beam, at a distance of 14.5 mm from the beam, and are opposite to each other. The solid angle subtended by each detector is 0.64 sr. The photon detectors are labeled c and d and their directions are expressed by the angles Θ_c and Θ_d, respectively, which are measured from the unit polarization vector of the incident light $\hat{\varepsilon}$. The positive direction of the angles Θ_c and Θ_d is counterclockwise when facing into the incident light beam. In the present experiment, the angles Θ_c and Θ_d were fixed to be -90° and 90°, respectively, i.e., the arrangement in Fig. 4(d).

Recently, false coincidence signals originating from cosmic muons in the present apparatus were reported by Nakanishi *et al.* [21], the count rate of which is 0.4×10^{-3} to 1.2×10^{-3} cps. In the present experiment false coincidences due to cosmic muons were not subtracted because the ratio of false coincidence counts to real coincidence counts was less than 5% even at the tail of the cross-section curve.

The two-photon coincidence count rate, $\dot{N}_{cd}(E,\Theta_c,\Theta_d)$, at a given energy of incident photon, E, and at given angles of detectors, Θ_c and Θ_d, is related to the cross section for emission of a pair of Lyman-α photons differential with respect to the solid angles of emitted photons, $q(E,\Theta_c,\Theta_d)$, as

$$\dot{N}_{cd}(E,\Theta_c,\Theta_d)=2n\left(\frac{I'(E)G_{cd}(\Theta_c,\Theta_d)}{A}\right)\eta_{cd}\langle q\rangle(E,\Theta_c,\Theta_d), \tag{2}$$

where $\langle q\rangle(E,\Theta_c,\Theta_d)$ is the angle-differential cross section averaged with the angular resolution, which is to be measured, n the number density of target molecules, $I'(E)$ the flux of incident photons, A the cross-section area of the incident photon beam, $G_{cd}(\Theta_c,\Theta_d)$ the geometric factor, and η_{cd} the coincidence detection efficiency of the photon detectors for the Lyman-α photons. The geometric factor $G_{cd}(\Theta_c,\Theta_d)$ is in fact independent of (Θ_c,Θ_d) as discussed in Ref. [21]. It is also independent of the incident photon energy E since the position and shape of the incident light beam do not change quite as much in the present range of incident photon energy. For the same reason, A is independent of E. The flux of incident photons, $I'(E)$, is related to the photocurrent of the Au plate, $i_{\rm Au}(E)$, as

$$I'(E)=CK(E)i_{\rm Au}(E), \tag{3}$$

where C is a constant independent of E. The function $K(E)$, which is related to the sensitivity of the Au plate as a function of the incident photon energy, is obtained with successive measurements of photocurrents of the Au plate and silicon photodiode [23]. The sensitivity of the latter was provided by NIST. We found a decrease in the sensitivity of the silicon photodiode under irradiation of the incident light during the coincidence measurements, while this decrease in sensitivity was not observed for the Au plate. This is why the flux of incident photons was measured using not the silicon photodiode, but the Au plate.

According to Eqs. (2) and (3), the coincidence count rate $\dot{N}_{cd}$ is normalized for the target gas pressure and flux of incident photons,

$$S_{cd}(E,\Theta_c,\Theta_d)=\frac{\dot{N}_{cd}(E,\Theta_c,\Theta_d)}{P[K(E)i_{\rm Au}(E)]}, \tag{4}$$

where P is the pressure of molecular hydrogen or deuterium in the gas cell. The plot of the values of $S_{cd}(E,\Theta_c,\Theta_d)$ against the incident photon energy E with the angles Θ_c and Θ_d held fixed shows a plot of the cross section $\langle q\rangle(E,\Theta_c,\Theta_d)$ against E on a relative scale of the vertical axis. However, in fact, reference measurements were carried out at a constant energy of the incident photon, E^{Ref}, to compensate a possible but small and slow change of the geometric factor $G_{cd}(\Theta_c,\Theta_d)$, the sensitivity of the detectors η_{cd}, the cross-section area A, and the factor C in Eqs. (2) and (3) during the coincidence measurement. Reference measurements were carried out before and after the measurement of $\dot{N}_{cd}(E,\Theta_c,\Theta_d)$ to obtain $\dot{N}^b_{cd}(E^{\mathrm{Ref}},\Theta_c,\Theta_d)$ and $\dot{N}^a_{cd}(E^{\mathrm{Ref}},\Theta_c,\Theta_d)$, respectively. In the present experiment, the values of

$$\frac{S_{cd}(E,\Theta_c,\Theta_d)}{\frac{1}{2}\left[S^b_{cd}(E^{\mathrm{Ref}},\Theta_c,\Theta_d)+S^a_{cd}(E^{\mathrm{Ref}},\Theta_c,\Theta_d)\right]} = \frac{\langle q\rangle(E,\Theta_c,\Theta_d)}{\langle q\rangle(E^{\mathrm{Ref}},\Theta_c,\Theta_d)} \tag{5}$$

measured at given Θ_c and Θ_d are plotted against E to show the relative values of $\langle q\rangle(E,\Theta_c,\Theta_d)$ against E. The angles Θ_c and Θ_d were fixed to be -90° and 90°, respectively, in the present experiment as mentioned. The value of E^{Ref} was chosen to be 33.66 eV for H_2 and D_2, around which $\langle q\rangle(E,\Theta_c=-90^\circ,\Theta_d=90^\circ)$ for H_2 gives the maximum. The coincidence count rates for H_2 and D_2 at E^{Ref}, i.e., $\dot{N}^{H_2}_{cd}(E^{\mathrm{Ref}},\Theta_c,\Theta_d)$ and $\dot{N}^{D_2}_{cd}(E^{\mathrm{Ref}},\Theta_c,\Theta_d)$, respectively, were sequentially measured to obtain the ratio of $\langle q^{H_2}\rangle(E^{\mathrm{Ref}},\Theta_c,\Theta_d)$ and $\langle q^{D_2}\rangle(E^{\mathrm{Ref}},\Theta_c,\Theta_d)$. Eventually we plotted the relative values of $\langle q^{H_2}\rangle(E,\Theta_c,\Theta_d)$ and $\langle q^{D_2}\rangle(E,\Theta_c,\Theta_d)$, the angle-differential cross sections for H_2 and D_2, respectively, on the same scale of the vertical axis.

III. RESULTS AND DISCUSSION

A. Absolute values of the cross section for formation of a 2*p* atom pair against the incident photon energy

In Fig. 5, the relative values of $\langle q\rangle(E,\Theta_c=-90^\circ,\Theta_d=90^\circ)$ for H_2 measured in the present experiment are shown against the incident photon energy, E, together with those of $\langle q\rangle(E,\Theta_c=0^\circ,\Theta_d=180^\circ)$ for H_2 obtained by Odagiri *et al.* [18]. The error bars in both experiments show the statistical uncertainty. The angles of $\Theta_c=-90^\circ$ and $\Theta_d=90^\circ$ give the arrangement in Fig. 4(d) and those of $\Theta_c=0^\circ$ and $\Theta_d=180^\circ$ give the arrangement in Fig. 4(b). The present and previous results are normalized at the incident photon energy of 33.66 eV. The shapes of the cross-section curves are in good agreement with each other in the range lower than 36 eV. The small discrepancy seen above 36 eV seems to be due to the difference in the methods of measuring the flux of the incident photon beam, not due to the difference in angles of (Θ_c,Θ_d). The present method is better than the previous one as mentioned in Sec. II. In addition, the statistical uncertainty is much better than that in the previous experiment [18], which is attributed to the enhanced sensitivity of the microchannel plate due to the CsI coating.

In Fig. 6 the relative values of $\langle q\rangle(E,\Theta_c=-90^\circ,\Theta_d=90^\circ)$ for H_2 and D_2 measured in the present experiment are shown against the incident photon energy E, where the scale

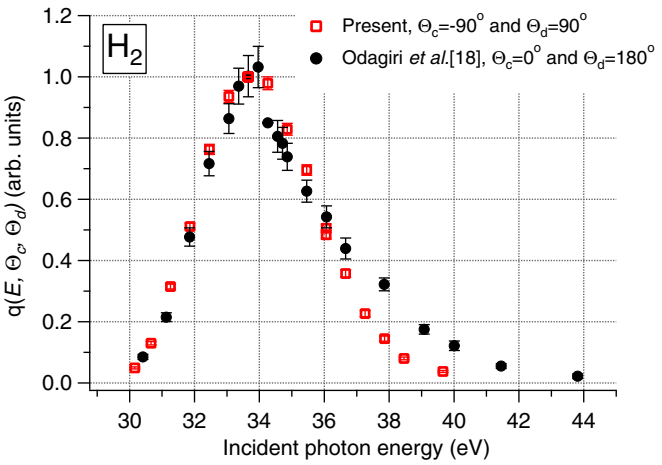

FIG. 5. Relative values of $\langle q\rangle(E,\Theta_c,\Theta_d)$ of H_2 against the incident photon energy E. Open squares: present results measured at $\Theta_c=-90^\circ$ and $\Theta_d=90^\circ$. Filled circles: results measured by Odagiri *et al.* [18] at $\Theta_c=0^\circ$ and $\Theta_d=180^\circ$. Both cross sections are normalized at 33.66 eV.

of the vertical axis is the same for H_2 and D_2. The slightly higher peak energy in the D_2 curve and narrower width at the bottom of the D_2 curve are probably attributable to the decrease in the zero-point energy in the ground electronic state of the hydrogen molecule, the $X\,^1\Sigma_g^+$ state, caused by the heavier isotope substitution: the zero-point energy in D_2 is lower than that in H_2 by 80 meV [28]. The decrease in the zero-point

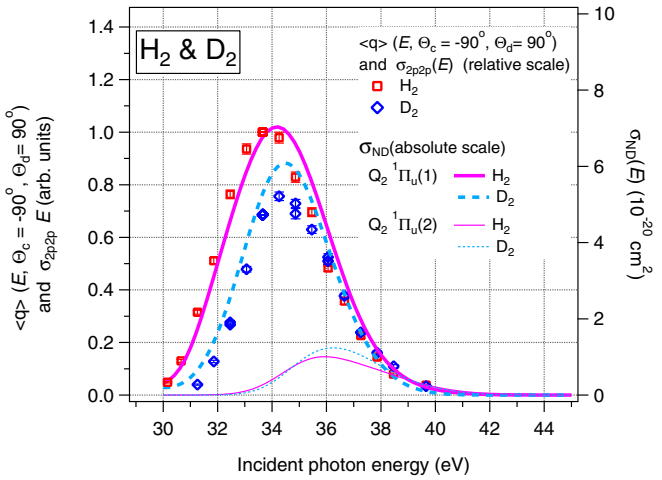

FIG. 6. Relative values of $\langle q\rangle(E,\Theta_c=-90^\circ,\Theta_d=90^\circ)$ as a function of the incident photon energy E. Open squares, H_2; open diamonds, D_2. The scale of the vertical axis is the same for H_2 and D_2. Thick curves show the theoretical cross sections of neutral dissociation σ_{ND} in photoexcitation to the $Q_2\,^1\Pi_u(1)$ state of H_2 and D_2. Thick solid curve, H_2; thick dashed curve, D_2 [25–27]. Thin curves show the theoretical cross sections of neutral dissociation σ_{ND} in photoexcitation to the $Q_2\,^1\Pi_u(2)$ state of H_2 and D_2. Thin solid curve, H_2; thin dotted curve, D_2 [25–27]. Absolute values of σ_{ND} are shown on the right axis. The experimental cross sections of H_2 (open squares) have been fitted to the theoretical curve of photoexcitation to the $Q_2\,^1\Pi_u(1)$ state of H_2 (thick solid curve), keeping the relation between the experimental cross section of H_2 and that of D_2.

energy results in a narrower Franck-Condon region in D_2 than in H_2 as shown in Fig. 1(a).

In Fig. 6 the results of the present experiment are compared with the theoretical cross sections of neutral dissociation in photoexcitation to the $Q_2\,^1\Pi_u(1)$ and $Q_2\,^1\Pi_u(2)$ states obtained by solving the time-dependent Schrödinger equation for H_2 and D_2 molecules under a photon field [25–27]. Neutral dissociation in the theory means that a doubly excited hydrogen molecule dissociates down its potential energy curve into a pair of hydrogen atoms escaping from autoionization. The nonadiabatic transition is not considered in the theory. The theoretical cross section of neutral dissociation in photoexcitation to the $Q_2\,^1\Pi_u(1)$ state is much larger than that in photoexcitation to the $Q_2\,^1\Pi_u(2)$ state. The experimental cross sections of H_2, $\langle q\rangle(E, \Theta_c = -90^\circ, \Theta_d = 90^\circ)$, are fitted to the theoretical cross section of neutral dissociation in photoexcitation to the $Q_2\,^1\Pi_u(1)$ state of H_2 in Fig. 6, keeping the relation between the experimental cross sections of H_2 and D_2. It is shown that the experimental curves of H_2 and D_2 are in good agreement with the theoretical curves of neutral dissociation in photoexcitation to the $Q_2\,^1\Pi_u(1)$ state of H_2 and D_2, respectively, in terms of shape. A better fitting is not obtained if the contribution of the $Q_2\,^1\Pi_u(2)$ state is added, since including the $Q_2\,^1\Pi_u(2)$ state shifts the peak consisting of the theoretical $Q_2\,^1\Pi_u(1)$ and $Q_2\,^1\Pi_u(2)$ curves to the higher energy side. It is hence concluded from the shape of the experimental and theoretical curves that the pair of $2p$ atoms is produced from the $Q_2\,^1\Pi_u(1)$ state in the photoexcitation of H_2 and D_2 and the contribution of the $Q_2\,^1\Pi_u(2)$ state is negligible in H_2 and D_2. This is consistent with the assignment of the precursor doubly excited state of the $2p$ atom pair in the photoexcitation of H_2 by Odagiri *et al.* [18], who reached the same assignment using the cross sections of neutral dissociation calculated with the reflection approximation and semiclassical treatment of the decay of doubly excited states as mentioned in Sec. I.

The relative values of $\langle q\rangle(E, \Theta_c = -90^\circ, \Theta_d = 90^\circ)$ against E in Fig. 6 are considered those of the angle-integrated cross sections of $2p$ atom pair formation against E as mentioned below. The angular correlation function of a pair of Lyman-α photons in the photoexcitation of H_2 [29] appears to be independent of the incident photon energy in the present range since only the $Q_2\,^1\Pi_u(1)$ state contributes to the formation of the $2p$ atom pair. The energy-independent angular correlation seems also to be the case in D_2. The angular correlation function of a pair of Lyman-α photons in the photoexcitation of H_2 was measured at 33.66-eV incident photon energy for the arrangements with $\Theta_d = \Theta_c + 180^\circ$, $\Theta_d = -\Theta_c$, and $\Theta_d = -\Theta_c + 180^\circ$ and it was found that the angular correlation is not quite as strong [21]. The angular correlation function in the photoexcitation of D_2 was preliminarily measured at 34.86-eV incident photon energy for the arrangement with $\Theta_d = \Theta_c + 180^\circ$ [30]. The angular correlation function in H_2 at 33.66 eV for the arrangement with $\Theta_d = \Theta_c + 180^\circ$ is in good agreement with the angular correlation function in D_2 at 34.86 eV for the arrangement with $\Theta_d = \Theta_c + 180^\circ$. In conclusion, the angular correlation functions of a pair of Lyman-α photons in the photoexcitation of H_2 and D_2 appear to be independent of the incident photon energy in the present range and the isotope effect on the angular correlation function seems small. It hence follows that the experimental $\langle q\rangle(E, \Theta_c = -90^\circ, \Theta_d = 90^\circ)$ on the same relative scale of the vertical axis for H_2 and D_2 in Fig. 6 is considered the angle-integrated cross section of $2p$ atom pair formation, $\sigma_{2p2p}(E)$, on the same relative scale for H_2 and D_2. This is why the vertical axis in Fig. 6 is labeled $\sigma_{2p2p}(E)$ in addition to $\langle q\rangle(E, \Theta_c = -90^\circ, \Theta_d = 90^\circ)$.

Before plotting the relative values of $\sigma_{2p2p}(E)$ in Fig. 6 on the absolute scale, we discuss the dissociation pairs produced from the $Q_2\,^1\Pi_u(1)$ state other than the $2p$ atom pair and then derive Eqs. (6) and (7), on which our procedure for plotting the values on the absolute scale relies. Odagiri *et al.* [19] measured the symmetry-resolved cross sections of $2s$ atom formation in photoexcitation to the Σ and Π states of H_2 and D_2 against the incident photon energy. They obtained the absolute values of the cross section by normalizing the sum of their relative values of the symmetry-resolved cross sections to the absolute values of the symmetry-unresolved cross sections obtained by Glass-Maujean *et al.* [31]. Odagiri *et al.*[19] pointed out a large contribution of the $Q_2\,^1\Pi_u(1)$ state to the formation of the $2s$ atom. The $Q_2\,^1\Pi_u(1)$ state of H_2 and D_2 also yields the pair of $2p$ atoms as mentioned before. Let us determine the partner of the $2s$ atom in photoexcitation to the $Q_2\,^1\Pi_u(1)$ state. There are four candidates, i.e., the $n\ell$ atom ($n \geqslant 3$), $1s$ atom, $2s$ atom, and $2p$ atom.

A contribution of the $Q_2\,^1\Pi_u(1)$ state is not seen in cross sections for emission of Balmer-α fluorescence against the incident photon energy in the photoexcitation of H_2 [4,32,33]. The possibility of the first candidate is hence eliminated. The $Q_2\,^1\Pi_u(1)$ state is also unlikely to result in the formation of $H(nl) + H(1s)$ $[D(nl) + D(1s)]$ pair, where the principal quantum number $n \geqslant 2$. The reason is as follows. The nonadiabatic transition from the $Q_2\,^1\Pi_u(1)$ state to Q_1 states, which result in the formation of a $H(nl) + H(1s)$ $[D(nl) + D(1s)]$ pair, seems not to occur in the range of the incident photon energy below approximately 35.5 eV in H_2 and D_2 since the potential energy curve of the $Q_2\,^1\Pi_u(1)$ state is above that of the $2p\sigma_u$ state, the ion core state of the Q_1 states, as shown in Fig. 1 (a), and thus does not become close to the potential energy curves of the Q_1 states. On the other hand, in the range of the incident photon energy above approximately 35.5 eV, there is a possibility that the $Q_2\,^1\Pi_u(1)$ state contributes to the formation of the $H(nl) + H(1s)$ $[D(nl) + D(1s)]$ pair through nonadiabatic transition to Q_1 states. However, no break is seen around 35.5 eV in the experimental cross sections of $2p$ atom pair formation in Fig. 6. The $Q_2\,^1\Pi_u(1)$ state hence seems not to result in the formation of a $H(nl) + H(1s)$ $[D(nl) + D(1s)]$ pair. The possibility of the second candidate, the $1s$ atom, is eliminated.

One $^1\Sigma_g^+$ state and one $^3\Sigma_u^+$ state result from the $2s + 2s$ pair following the building-up principle [34], and the $^1\Pi_u$ state does not transfer to either the $^1\Sigma_g^+$ state or the $^3\Sigma_u^+$ state through nonadiabatic coupling. The $Q_2\,^1\Pi_u(1)$ state hence does not lead to the formation of a $2s + 2s$ pair. The possibility of the third candidate, the $2s$ atom, is eliminated.

It follows that none of the first three candidates, the $n\ell$ atom ($n \geqslant 3$), $1s$ atom, or $2s$ atom, can be a partner of the $2s$ atom in photoexcitation to the $Q_2\,^1\Pi_u(1)$ state, and hence the $2p$ atom is a partner of the $2s$ atom. In addition,

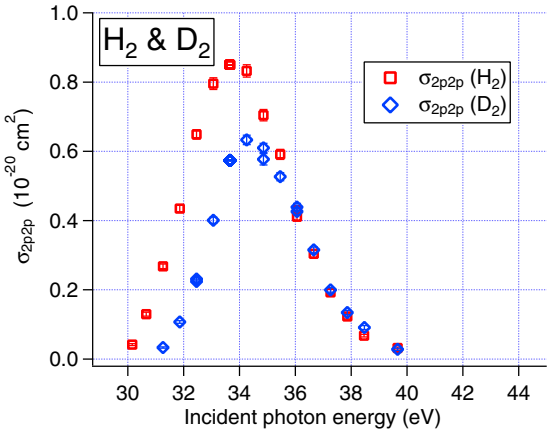

FIG. 7. Absolute values of the cross sections of $2p$ atom pair formation in the photoexcitation of H_2 (open squares) and D_2 (open diamonds) against the incident photon energy.

we conclude from the above discussion that a hydrogen or deuterium molecule excited to the $Q_2\,{}^1\Pi_u(1)$ state mainly dissociates into a $2s+2p$ pair or $2p+2p$ pair. The following equations for the oscillator strengths of dissociation processes from the $Q_2\,{}^1\Pi_u(1)$ state are hence obtained for H_2 and D_2:

$$f_{2s}(Q_2\,{}^1\Pi_u(1)) = f_{2s2p}(Q_2\,{}^1\Pi_u(1)), \tag{6}$$

$$f_{2p}(Q_2\,{}^1\Pi_u(1)) = f_{2s2p}(Q_2\,{}^1\Pi_u(1)) + 2f_{2p2p}(Q_2\,{}^1\Pi_u(1)), \tag{7}$$

where $f_{2s}(Q_2\,{}^1\Pi_u(1))$ is the oscillator strength of $2s$ atom formation, $f_{2p}(Q_2\,{}^1\Pi_u(1))$ the oscillator strength of $2p$ atom formation, $f_{2s2p}(Q_2\,{}^1\Pi_u(1))$ the oscillator strength of $2s+2p$ pair formation, and $f_{2p2p}(Q_2\,{}^1\Pi_u(1))$ the oscillator strength of $2p+2p$ pair formation: the precursor state is the $Q_2\,{}^1\Pi_u(1)$ state in all cases. The oscillator strength of each process is obtained by integrating the cross-section curve of each process [see Eq. (11)].

The quantum yields of H($2s$) formation and H($2p$) formation from the $Q_2\,{}^1\Pi_u(1)$ state of H_2 were derived [4] based on the experimental cross sections of H($2s$) formation and H($2p$) formation against the incident photon energy in the photoexcitation of H_2 [31,35]. According to the quantum yields [4], the ratio of $f_{2p}(Q_2\,{}^1\Pi_u(1))/f_{2s}(Q_2\,{}^1\Pi_u(1))$ in H_2 is obtained as

$$\frac{f_{2p}(Q_2\,{}^1\Pi_u(1))}{f_{2s}(Q_2\,{}^1\Pi_u(1))} = \frac{f_{2p}(Q_2\,{}^1\Pi_u(1))}{f_{2s2p}(Q_2\,{}^1\Pi_u(1))} = \frac{0.12}{0.09}. \tag{8}$$

Substituting Eq. (8) into Eq. (7) we obtain

$$f_{2p2p}(Q_2\,{}^1\Pi_u(1)) = 0.17\,f_{2s2p}(Q_2\,{}^1\Pi_u(1)) \tag{9}$$

for H_2. The relative scale of $\sigma_{2p2p}(E)$ for H_2 and D_2 in Fig. 6 is converted to the absolute scale using Eq. (9) for H_2 since the absolute value of $f_{2s2p}(Q_2\,{}^1\Pi_u(1))$ for H_2 is known [19]. The derivation of Eq. (9) for H_2 plays a significant role in obtaining the absolute values of $\sigma_{2p2p}(E)$ for H_2 and D_2. The absolute values of the cross sections of $2p$ atom pair formation in the photoexcitation of H_2 and D_2, $\sigma_{2p2p}(E)$, are shown against the incident photon energy in Fig. 7.

We calculated the value of $S_{cd}(E = 33.66\text{ eV}, \Theta_c = -90^\circ, \Theta_d = 90^\circ)$ for D_2 defined in Eq. (4) from the absolute value of $\sigma_{2p2p}(E = 33.66\text{ eV})$ for D_2 in Fig. 7 together with the simulated value of $G_{cd}(\Theta_c = -90^\circ, \Theta_d = 90^\circ)/A$ in Eq. (2) and expected values of η_{cd} in Eq. (2) and C in Eq. (3). The angle-differential cross section $\langle q\rangle(E = 33.66\text{ eV}, \Theta_c = -90^\circ, \Theta_d = 90^\circ)$ in Eq. (2) was approximated as

$$\langle q\rangle(E = 33.66\text{ eV}, \Theta_c = -90^\circ, \Theta_d = 90^\circ) = \frac{1}{(4\pi)^2}\sigma_{2p2p}(E = 33.66\text{ eV}) \tag{10}$$

since Nakanishi *et al.* [21] measured the angular correlation function of a pair of Lyman-α photons in the photoexcitation of H_2 at $E = 33.66$ eV to find that the angular correlation is not quite as strong and the isotope effect on the angular correlation function seems small as mentioned. The calculated S_{cd} is compared with the experimental one to show the validity of the absolute values in Fig. 7. The calculated and experimental values of $S_{cd}(E = 33.66\text{ eV}, \Theta_c = -90^\circ, \Theta_d = 90^\circ)$ for D_2 are in agreement with each other within factors of about three or less, indicating that the absolute values of $\sigma_{2p2p}(E)$ in Fig. 7 are reasonable. We note that only one standard was used in the process of obtaining the absolute values of $\sigma_{2p2p}(E)$ in Fig. 7, which is the set of the absolute cross sections of H($2s$) formation and H($2p$) formation in the photoexcitation of H_2 against the incident photon energy obtained by Glass-Maujean *et al.* [31].

B. Dynamics of the doubly excited $Q_2\,{}^1\Pi_u(1)$ state

We discuss the dynamics of the doubly excited $Q_2\,{}^1\Pi_u(1)$ state, the precursor doubly excited state of the $2p+2p$ pair and $2s+2p$ pair, in terms of the isotope effect on the oscillator strength of each channel in photoexcitation. The cross section of channel j in photoexcitation by a photon of energy E, $\sigma_j(E)$, is related to the density of the oscillator strength of channel j per unit range of energy E, df_j/dE, by

$$\sigma_j(E) = 4\pi^2\alpha a_0^2\frac{df_j}{d(E/R)}, \tag{11}$$

where α is the fine-structure constant, R the Rydberg energy, and a_0 the Bohr radius [36]. Equation (11) is more conveniently written as

$$\sigma_j(E) = 1.098\times10^{-16}\left(\frac{df_j}{dE}\right), \tag{12}$$

where $\sigma_j(E)$ is expressed in cm^2 and df_j/dE in eV^{-1}. The integration of df_j/dE originating from the electronic state s over the range of E gives the oscillator strength of channel j from state s, $f_j(s)$. Thus the integration of the experimental cross sections of $2p$ atom pair formation for H_2 and D_2 in Fig. 7 gives the oscillator strengths of $2p$ atom pair formation for H_2 and D_2 from the $Q_2\,{}^1\Pi_u(1)$ state, $f^{H_2}_{2p2p}(Q_2\,{}^1\Pi_u(1))$ and $f^{D_2}_{2p2p}(Q_2\,{}^1\Pi_u(1))$, respectively, as listed in Table I [the value of $f^{H_2}_{2p2p}(Q_2\,{}^1\Pi_u(1))$ is equal to that obtained from Eq. (9)]. Also listed are the experimental oscillator strengths of the formation of the $2s+2p$ pair for H_2 and D_2 from the $Q_2\,{}^1\Pi_u(1)$ state, $f^{H_2}_{2s2p}(Q_2\,{}^1\Pi_u(1))$ and $f^{D_2}_{2s2p}(Q_2\,{}^1\Pi_u(1))$, respectively, obtained by our group [19]. The theoretical oscillator strengths

TABLE I. Experimental oscillator strengths of $2p+2p$ pair formation from the $Q_2\,^1\Pi_u(1)$ state, $f_{2p2p}(Q_2\,^1\Pi_u(1))$, in the photoexcitation of H_2 and D_2 together with experimental oscillator strengths of $2s+2p$ pair formation from the $Q_2\,^1\Pi_u(1)$ state, $f_{2s2p}(Q_2\,^1\Pi_u(1))$. The theoretical oscillator strengths of neutral dissociation from the $Q_2\,^1\Pi_u(1)$ state, $f_{\rm ND}^{\rm th}(Q_2\,^1\Pi_u(1))$, in the photoexcitation of H_2 and D_2 are also listed. The ratio of the oscillator strength of D_2 to that of H_2 for each channel is listed.

	H_2	D_2	f^{D_2}/f^{H_2}
$f_{2p2p}(Q_2\,^1\Pi_u(1))$	3.5×10^{-4}	2.4×10^{-4}	0.69
$f_{2s2p}(Q_2\,^1\Pi_u(1))$ [19]	21×10^{-4}	14×10^{-4}	0.67
$f_{\rm ND}^{\rm th}(Q_2\,^1\Pi_u(1))$ [25–27]	31×10^{-4}	23×10^{-4}	0.76

of neutral dissociation for H_2 and D_2 from the $Q_2\,^1\Pi_u(1)$ state, $f_{\rm ND}^{\rm th,H_2}(Q_2\,^1\Pi_u(1))$ and $f_{\rm ND}^{\rm th,D_2}(Q_2\,^1\Pi_u(1))$, respectively, are obtained by integrating the thick curves in Fig. 6 [25–27], and the values are listed in Table I.

A clear isotope effect, f^{D_2}/f^{H_2}, for the experimental $f_{2p2p}(Q_2\,^1\Pi_u(1))$, in addition to that for the experimental $f_{2s2p}(Q_2\,^1\Pi_u(1))$, is reported in Table I: the heavier isotope substitution brings about the smaller oscillator strengths. Such isotope effects are explained as the result of the competition between electronic autoionization and neutral dissociation. The potential energy curve and resonance width of a doubly excited state have no isotope effects, and the latter gives the rate of electronic autoionization. On the other hand, the relative velocity of two nuclei down the potential energy curve in D_2 is $1/\sqrt{2}$ that in H_2, and thus D_2 needs more time to reach the region of the internuclear distance of 0 or a small resonance width than H_2. As a result, D_2 has a lower probability of escaping from autoionization than H_2. The oscillator strength of the electronic excitation has just a small isotope effect since the sum of the Franck-Condon factors of the electronic excitation is equal to unity. In fact the calculated oscillator strengths of the excitation $X\,^1\Sigma_g^+ v=0 \rightarrow B\,^1\Sigma_u^+$ and the excitation $X\,^1\Sigma_g^+ v=0 \rightarrow C\,^1\Pi_u$ in H_2 are equal to those in HD and D_2 within the accuracy of the calculation [37], where v is the vibrational quantum number, and the calculated values for H_2 are in good agreement with the experimental ones [38] for H_2. Thus, in general, the state-resolved oscillator strength of neutral dissociation in D_2 is smaller than that in H_2 and the state-resolved oscillator strength of autoionization in D_2 is larger than that in H_2. The experimental isotope effects on the oscillator strengths of $2p+2p$ pair formation and $2s+2p$ pair formation from the $Q_2\,^1\Pi_u(1)$ state reflect the competition between neutral dissociation and autoionization.

We discuss the isotope effects on $f_{2p2p}(Q_2\,^1\Pi_u(1))$ and $f_{2s2p}(Q_2\,^1\Pi_u(1))$ in Table I in more detail. The adiabatic correlation diagram of the $Q_2\,^1\Pi_u(1)$ and $Q_2\,^1\Pi_u(2)$ states [19] is shown in Fig. 8. There is an avoided crossing between the potential energy curves of the $Q_2\,^1\Pi_u(1)$ and $Q_2\,^1\Pi_u(2)$ states at the internuclear distance of ~5.6 a.u. [9] as shown schematically in Fig. 8. A hydrogen molecule excited to the $Q_2\,^1\Pi_u(1)$ state in the Franck-Condon region leads to either a $2p+2p$ pair or a $2s+2p$ pair through nonadibatic coupling at ~5.6 a.u. as shown by arrows in Fig. 8. It is remarkable that the isotope effects on $f_{2p2p}(Q_2\,^1\Pi_u(1))$ and $f_{2s2p}(Q_2\,^1\Pi_u(1))$ are

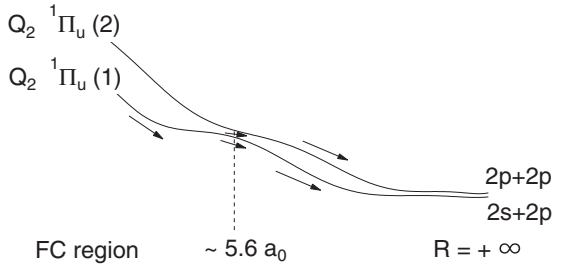

FIG. 8. Adiabatic correlation diagram of the doubly excited $Q_2\,^1\Pi_u(1)$ and $Q_2\,^1\Pi_u(2)$ states of H_2 and D_2, which shows the correlation between the electronic states in the Franck-Condon (FC) region and those at an infinite internuclear distance. The avoided crossing is seen at the internuclear distance of ~5.6 a.u. [9]. Reproduced from Ref. [19].

almost the same. This result shows that the isotope effects on the oscillator strengths of both channels are dominated by the potential energy curve and resonance width of the $Q_2\,^1\Pi_u(1)$ state before the doubly excited molecule in the $Q_2\,^1\Pi_u(1)$ state reaches the branching point into $2p+2p$ pair formation and $2s+2p$ pair formation, ~5.6 a.u. It is reasonable that the dynamics of the $Q_2\,^1\Pi_u(1)$ state before reaching the branching point dominate the isotope effects since the early population of the $Q_2\,^1\Pi_u(1)$ state is larger than the populations of the $Q_2\,^1\Pi_u(1)$ and $Q_2\,^1\Pi_u(2)$ states after passage of the branching point. In this context, we compare the experimental isotope effects with the isotope effect on the survival probabilities of the $Q_2\,^1\Pi_u(1)$ state, $s(Q_2\,^1\Pi_u(1))$, during movement from the equilibrium internuclear distance, 1.4 a.u., to the branching point [14]. In the calculation of the survival probabilities the nuclear motion is treated in a classical manner [39]. The isotope effect on the survival probabilities is equal to the isotope effect on the oscillator strengths of the process that the molecule in the $Q_2\,^1\Pi_u(1)$ state survives at the branching point since the oscillator strength of the electronic excitation has just a small isotope effect as mentioned before. The calculated ratio $s^{D_2}(Q_2\,^1\Pi_u(1))/s^{H_2}(Q_2\,^1\Pi_u(1))$ is 0.60, which is in agreement with the isotope effects on the experimental oscillator strengths of $2p+2p$ pair formation and $2s+2p$ pair formation from the $Q_2\,^1\Pi_u(1)$ state as expected. The calculation of the survival probabilities supports our thoughts.

It is suggested that the nonadiabatic coupling at the internuclear distance of ~5.6 a.u. would not influence the isotope effects on $f_{2p2p}(Q_2\,^1\Pi_u(1))$ and $f_{2s2p}(Q_2\,^1\Pi_u(1))$ quite as much. In this respect, we compare the experimental isotope effects with the isotope effect on the theoretical oscillator strengths of neutral dissociation from the $Q_2\,^1\Pi_u(1)$ state [25–27] in Table I. The theoretical oscillator strengths were obtained by solving the time-dependent Schrödinger equation of H_2 and D_2 under a photon field. Neutral dissociation means that a doubly excited hydrogen molecule dissociates down its potential energy curve into a pair of hydrogen atoms escaping from autoionization. The nonadiabatic transition is not taken into account in the theory. As expected the isotope effects on the experimental oscillator strengths of $2p+2p$ pair formation and $2s+2p$ pair formation from the $Q_2\,^1\Pi_u(1)$ state are in agreement with the isotope effect on the theoretical oscillator strengths of neutral dissociation from the $Q_2\,^1\Pi_u(1)$

state without consideration of the nonadiabatic transition. In conclusion, the isotope effects on $f_{2p2p}(Q_2\,{}^1\Pi_u(1))$ and $f_{2s2p}(Q_2\,{}^1\Pi_u(1))$ are dominated by the dynamics of the doubly excited $Q_2\,{}^1\Pi_u(1)$ state before reaching the branching point.

IV. CONCLUSION

We have measured the absolute values of the cross section for formation of a $2p$ atom pair as a function of the incident photon energy in the range 30–40 eV in the photoexcitation of H_2 and D_2 by means of the coincidence detection of two Lyman-α photons. The cross-section curves are explained only by the contribution of the doubly excited $Q_2\,{}^1\Pi_u(1)$ state of H_2 and D_2. The oscillator strengths of $2p$ atom pair formation from the $Q_2\,{}^1\Pi_u(1)$ state in H_2 and D_2 have been obtained. We have compared the isotope effect on the oscillator strengths of $2p + 2p$ pair formation and the isotope effect on the oscillator strengths of $2s + 2p$ pair formation [19] from the $Q_2\,{}^1\Pi_u(1)$ state, to find that the isotope effects are almost independent of dissociation channels: D_2/H_2 for the $2p + 2p$ pair formation is 0.69 and D_2/H_2 for the $2s + 2p$ pair formation is 0.67. It is concluded that the isotope effects on the oscillator strengths of neutral dissociation channels are dominated by the early dynamics of the $Q_2\,{}^1\Pi_u(1)$ state before reaching the branching point into $2p + 2p$ pair formation and $2s + 2p$ pair formation.

ACKNOWLEDGMENTS

The authors thank Prof. J. L. Sanz-Vicario for sending us unpublished data. The experiment was carried out under the approval of the Photon Factory Program Advisory Committee for Proposal No. 2014G108. This work was supported by JSPS KAKENHI Grants No. 23350003, No. 24550013, and No. 15K05381.

[1] J. N. Bardsley, J. Phys. B **1**, 349 (1968).
[2] I. Sánchez and F. Martín, Phys. Rev. A **57**, 1006 (1998).
[3] N. Kouchi, M. Ukai, and Y. Hatano, J. Phys. B **30**, 2319 (1997).
[4] M. Glass-Maujean and H. Schmoranzer, J. Phys. B **38**, 1093 (2005).
[5] I. Sánchez and F. Martín, Phys. Rev. Lett. **79**, 1654 (1997).
[6] I. Sánchez and F. Martín, Phys. Rev. Lett. **82**, 3775 (1999).
[7] J. Tennyson, At. Data Nucl. Data Tables **64**, 253 (1996).
[8] I. Sánchez and F. Martín, J. Chem. Phys. **106**, 7720 (1997).
[9] I. Sánchez and F. Martín, J. Chem. Phys. **110**, 6702 (1999).
[10] J. Fernández and F. Martín, J. Phys. B **34**, 4141 (2001).
[11] Y. V. Vanne, A. Saenz, A. Dalgarno, R. C. Forrey, P. Froelich, and S. Jonsell, Phys. Rev. A **73**, 062706 (2006).
[12] A. Igarashi and Y. Kuwayama, J. Phys. Soc. Jpn. **83**, 054302 (2014).
[13] T. Odagiri, N. Uemura, K. Koyama, M. Ukai, N. Kouchi, and Y. Hatano, J. Phys. B **29**, 1829 (1996).
[14] N. Uemura, T. Odagiri, T. Hirano, Y. Makino, N. Kouchi, and Y. Hatano, J. Phys. B **31**, 5183 (1998).
[15] F. Martín, J. Phys. B **32**, L181 (1999).
[16] L. Ishikawa, T. Odagiri, K. Yachi, N. Ohno, T. Tsuchida, M. Kitajima, and N. Kouchi, J. Phys. B **44**, 065203 (2011).
[17] T. E. Sharp, At. Data Nucl. Data Tables **2**, 119 (1970).
[18] T. Odagiri, M. Murata, M. Kato, and N. Kouchi, J. Phys. B **37**, 3909 (2004).
[19] T. Odagiri, Y. Kumagai, M. Nakano, T. Tanabe, I. H. Suzuki, M. Kitajima, and N. Kouchi, Phys. Rev. A **84**, 053401 (2011).
[20] K. Ito, Y. Morioka, M. Ukai, N. Kouchi, Y. Hatano, and T. Hayaishi, Rev. Sci. Instrum. **66**, 2119 (1995).
[21] Y. Nakanishi, K. Hosaka, R. Kougo, T. Odagiri, M. Nakano, Y. Kumagai, K. Shiino, M. Kitajima, and N. Kouchi, Phys. Rev. A **90**, 043405 (2014).
[22] H. A. Bethe and E. E. Salpeter, *Quantum Mechanics of One- and Two-Electron Atoms* (Plenum Press, New York, 1977), p. 266.
[23] Model AXUV-100G, IRD Inc.
[24] Model F4655-10, Hamamatsu Photonics.
[25] J. D. Bozek, J. E. Furst, T. J. Gay, H. Gould, A. L. D. Kilcoyne, J. R. Machacek, F. Martín, K. W. McLaughlin, and J. L. Sanz-Vicario, J. Phys. B **39**, 4871 (2006); **41**, 039801 (2008); **42**, 029801 (2009).
[26] J. L. Sanz-Vicario (private communication).
[27] J. L. Sanz-Vicario, H. Bachau, and F. Martín, Phys. Rev. A **73**, 033410 (2006).
[28] K. P. Huber and G. Herzberg, *Molecular Spectra and Molecular Structure, Vol. 6. Constants of Diatomic Molecules* (Van Norstrand Reinhold, New York, 1979), pp. 240–267.
[29] H. Miyagi, A. Ichimura, and N. Kouchi, J. Phys. B **40**, 617 (2007); K. Jänkälä, P. V. Demekhin, S. Heinäsmäki, I. Haar, R. Hentges, and A. Ehresmann, *ibid.* **43**, 065104 (2010).
[30] K. Hosaka (private communication).
[31] M. Glass-Maujean, S. Klumpp, L. Werner, A. Ehresmann, and H. Schmoranzer, J. Phys. B **37**, 2677 (2004).
[32] M. Glass-Maujean, H. Frohlich, and P. Martin, Phys. Rev. A **52**, 4622 (1995).
[33] E. M. García, J. Á. Ruiz, S. Menmuir, E. Rachlew, P. Erman, A. Kivimäki, M. Glass-Maujean, R. Richter, and M. Coreno, J. Phys. B **39**, 205 (2006).
[34] G. Herzberg, *Molecular Spectra and Molecular Structure*, Vol. 1. Spectra of Diatomic Molecules (D. Van Norstrand, Princeton, NJ, 1950), pp. 315–322.
[35] S. Arai, T. Yoshimi, M. Morita, K. Hironaka, T. Yoshida, H. Koizumi, K. Shinsaka, Y. Hatano, A. Yagishita, and K. Ito, Z. Phys. D **4**, 65 (1986).
[36] N. Kouchi and T. Odagiri, in *Charged Particle and Photon Interactions with Matter, Chemical, Physiochemical, and Biological Consequences with Applications*, edited by A. Mozumder and Y. Hatano (Marcel Dekker, New York, 2004), Chap. 5.
[37] A. C. Allison and A. Dalgarno, At. Data Nucl. Data Tables **1**, 289 (1970).
[38] W. F. Chan, G. Cooper, and C. E. Brion, Chem. Phys. **168**, 375 (1992).
[39] H. Nakamura, J. Phys. Soc. Jpn. **26**, 1473 (1969).